(Article begins on next page)

A revision of the conductive hearing loss in Cranium 4 from the Middle Pleistocene site of Sima de los Huesos (Burgos, Spain)

Mercedes Conde-Valverde[a,*], Manuel Rosa[a,b], Ignacio Martínez[a,c], Julio Marchamalo[a], Ana Pantoja-Pérez[c], Rolf Quam[a,c,d,e], Carlos Lorenzo[f,g], Ana Gracia-Téllez[c,h], Alfredo García-Fernández[a,i,j], Juan Luis Arsuaga [a,c,k], Teresa Rivera-Rodríguez[a,l,m,n]

[a] *Cátedra de Otoacústica Evolutiva y Paleoantropología (Hospitales Madrid-Universidad de Alcalá), Departamento de Ciencias de la Vida, Universidad de Alcalá, Campus Universitario, Ctra. Madrid-Barcelona km 33,600, 28871 Alcalá de Henares, Madrid, Spain*

[b] *Departamento de Teoría de la Señal y Comunicaciones, Escuela Politécnica Superior, Universidad de Alcalá, Campus Universitario, 28805 Alcalá de Henares, Spain*

[c] *Centro Mixto (UCM-ISCIII) de Evolución y Comportamiento Humanos, Av. Monforte de Lemos 5, 28029 Madrid, Spain*

[d] *Department of Anthropology, Binghamton University (SUNY) Binghamton, NY 13902-6000 USA*

[e] *Division of Anthropology, American Museum of Natural History, Central Park West-79th St., New York, NY 10024, USA*

[f] *Àrea de Prehistòria, Departament d'Història i Història de l'Art, Universitat Rovira i Virgili, Av. Catalunya 35, 43002 Tarragona, Spain*

[g] *Institut Català de Paleoecologia Humana i Evolució Social, Campus Sescelades URV, Zona Educacional 4, 43007 Tarragona, Spain*

[h] *Área de Paleontología, Departamento de Geografía y Geología, Facultad de Ciencias, Universidad de Alcalá, Campus Universitario, Ctra. Madrid-Barcelona km 33,600, 28871 Alcalá de Henares, Madrid, Spain*

[i] *Departamento de Ciencias Médicas Clínicas, Facultad de Medicina, Universidad CEU San Pablo, Urbanización Montepríncipe, 28925 Alcorcón, Madrid, Spain.*

[j] *Hospital Universitario HM Puerta del Sur, Avda. de Carlos V 70, 28938 Móstoles, Madrid, Spain.*

[k] *Departamento de Geodinámica, Estratigrafía y Paleontología, Facultad de Ciencias Geológicas, Universidad Complutense de Madrid, 28040 Madrid, Spain*

[l] *Servicio de Otorrinolaringología, Hospital Universitario Príncipe de Asturias, Ctra. Alcalá-Meco s/n, 28805 Alcalá de Henares, Madrid, Spain*

[m] *Departamento de Cirugía, Ciencias Morfológicas y Sociales, Facultad de Medicina, Universidad de Alcalá, Campus Universitario, Ctra. Madrid-Barcelona km 33,600, 28871 Alcalá de Henares, Madrid, Spain*

[n] *Centro de Investigación Biomédica en Red en enfermedades raras (Ciberer). Instituto de Salud Carlos III (ISCIII), Monforte de Lemos, 3-5, 28029, Madrid, Spain*

* Corresponding author.

E-mail address: mercedes.conde@fgua.es (M. Conde-Valverde).

Acknowledgments

The authors thank N. García, A. Aranburu and N. Sala for their valuable work at the Sima de los Huesos site. We also wish to thank P.J. Pérez for her pioneering work on the paleopathology of the Sima de los Huesos hominins. CT scanning of the SH fossils was carried out at the Laboratorio de la Evolución Humana (Burgos, Spain) by Rebeca García and Laura Rodríguez (Project No. BU005A09). The authors thank the associate editor and the three anonymous reviewers for their insightful and constructive comments on improving the manuscript. Financial support for this study was provided by the Ministerio de Economía y Competitividad of the Spanish Government (CGL2015-65387-C3-2-P) and Ministerio de Ciencia, Innovación y Universidades (PGC2018-093925-B-C33). M.C.V. and A.P.P. have received predoctoral grants from the Fundación Atapuerca. R.Q. has been supported by the Programa “Ginés de los Ríos” (Universidad de Alcalá). C.L. received financial support from the research project AGAUR 2017 SGR 1040. This paper forms part of the research carried out by the Evolutionary Bioacoustics Group at the Universidad de Alcalá (Spain).

A revision of the conductive hearing loss in Cranium 4 from the Middle Pleistocene site of Sima de los Huesos (Burgos, Spain)

Abstract

Pathological conditions have been previously documented in the Middle Pleistocene Sima de los Huesos hominins from northern Spain, and several of these have clear behavioral implications. Within this fossil assemblage, Cranium 4 shows bilateral external auditory exostoses which have been preliminarily interpreted as causing a significant hearing loss in this individual. If confirmed, this would be the oldest recorded case of deafness in human history and could have important implications for the antiquity of this condition, as well as social interactions. To further investigate this case, the current study presents 3D reconstructions of the entire outer and middle ear, based on computed tomography scans of both temporal bones in Cranium 4. We established the degree of stenosis in both external auditory canals, showing that in both cases the degree of stenosis is less than 52% of the original cross-sectional area of each canal. Based on clinical studies in living humans, the buildup of wax due to the degree of stenosis in Cranium 4 is unlikely to have caused frequent external ear infections. In addition, we estimated the pattern of sound power transmission up to 5 kHz in both ears relying on a comprehensive model developed in the bioengineering literature and which has been applied previously to the Sima de los Huesos hominins. The model was modified to account for the peculiar shape of the pathological external ear canals in Cranium 4. The results show that this pathology had little to no influence on the sound power transmission in this individual. Thus, we conclude that the exostoses present in both ears of Cranium 4 did not significantly affect their hearing.

Keywords: Atapuerca; External auditory exostoses; Stenosis; Deafness; Audition; Hominin

1. Introduction

The site of the Sima de los Huesos (SH) in the Sierra de Atapuerca (northern Spain) has yielded a large collection of Middle Pleistocene hominin remains. In addition to taxonomic and evolutionary questions relevant to understand the course of human evolution in the Middle

Pleistocene of Europe (Arsuaga et al., 2014, 2015), this collection has yielded multiple examples of pathological individuals (Pérez et al., 1997; Bonmatí et al., 2010; Gracia et al., 2009, 2010, 2012).

The study of pathological conditions in fossil skeletons can reveal insights into the health status, malnutrition, disease prevalence and trauma among fossil populations (Lovell, 1997, Wilbur et al., 2008). In addition, paleopathological studies can, on occasion, offer insights into more ephemeral aspects of human existence, including quality of life, cooperative relationships, social care/dependence, and compassion (Buikstra et al., 2010; Tilley and Oxenham, 2011; Coqueugniot et al., 2014).

Among the SH fossils, several examples of paleopathology have been previously reported, with clear behavioral implications. Cranium 14 represents an adolescent individual showing a clear case of craniosynostosis, resulting in cranial and cerebral asymmetries and likely some degree of cognitive impairment (Gracia et al., 2009, 2010). The survival of this individual into adolescence has been interpreted as evidence of social care in the past. Similarly, Cranium 5 represents an older adult individual showing pronounced orofacial lesions, including periapical abscesses and periostitis, which have been posited as the likely cause of death in this individual (Gracia et al.,2012). This condition would have been associated with some degree of pain and probably difficulties in mastication, again implying some degree of social care. Another old adult individual is represented by a nearly complete pelvis (Pelvis 1) and lumbar spine exhibiting several deformities, including spondylolisthesis and Baastrup disease (Bonmatí et al., 2010). These conditions had postural consequences and would have resulted in impaired movement. Finally, Cranium 17 shows two perimortem traumatic injuries on the frontal bone that have been interpreted as evidence of lethal interpersonal violence (Sala et al., 2015).

In addition to the well-documented conditions in these individuals, Cranium 4 (SH Cr. 4) was initially diagnosed as suffering from hyperostosis (bone spurs) in the external auditory canal (EAC) of both ears (Pérez et al., 1997). These bilaterally symmetrical hyperostoses consist of an extensive growth of the tympanic bone that projects inside the EAC, considerably narrowing its cross-section. Two different pathologies can lead to hyperostosis of the EAC: exostoses and osteomas. Exostosis is defined as bilateral and symmetrical bone regrowth

affecting exclusively the bony portion of the EAC (Michaels, 2006) and is usually found on the medial end of the posterior wall of the EAC. An osteoma is usually not bilateral, has a pedicular appearance and affects only a small area in the lateral end of EAC (Sheehy, 1958; Rhys-Evans and Cameron, 2017). Relying on these criteria the bilateral pathology of the EAC of SH Cr.4 was diagnosed as exostoses (Pérez et al., 1997).

Since severe exostosis can lead to infections of the ear due to the accumulation of cerumen (Kennedy, 1986) and can be associated with variable levels of hearing loss (Whitaker et al., 1998; Cooper et al., 2010; Walling and Dickson, 2012), it has been proposed that SH Cr.4 had some type of hearing loss in both ears (Pérez et al., 1997). This individual has been considered to represent the first documented case of deafness in human evolutionary history (Trinkaus and Villotte, 2017). In living humans, hearing loss has clear social consequences since it is associated with delays in language acquisition, increased behavior problems, and psychological stress (Calderon and Greenberg, 2003; Stevenson et al., 2010).

The presence of external auditory exostoses is known in other human fossils of the Middle and Late Pleistocene, including *Homo neanderthalensis* and *Homo sapiens* (Trinkaus and Villotte, 2017; Trinkaus and Wu, 2017). The in-depth study of the external auditory exostoses present in both external auditory canals of the Shanidar 1 Neandertal specimen has led to the proposition that this individual was "effectively deaf in his right ear, and likely had at least partial CHL [conductive hearing loss] in the left ear" (Trinkaus and Villotte, 2017: 4). Additionally, in their exhaustive study on the presence of external auditory exostoses in eastern Asian Middle Pleistocene archaic *Homo*, Trinkaus and Wu (2017) proposed that both individuals from Xuchang (Xuchang 1 and 2) would have suffered CHL, although to a lesser extent in Xuchang 1. The presence of CHL in the SH Cr.4, Shanidar 1 and the two individuals from Xuchang has been presented as an argument in favor of social care in Middle and Late Pleistocene populations (Trinkaus and Villotte, 2017; Trinkaus and Wu, 2017).

The initial diagnosis of stenosis (narrowing) in SH Cr.4 was based on the visual inspection of the EAC and a single tomographic image of the left canal showing that it was almost fully occluded (Pérez et al., 1997). To further evaluate this preliminary suggestion, we have virtually reconstructed the outer and middle ears in SH Cr. 4 from high-resolution computed tomography (CT) scans and precisely measured the degree of stenosis along the

entire length of the EAC in both ears. Subsequently, we have reconstructed the sound power transmission through the outer and middle ear in the SH hominins (Cr.3, Cr.4, Cr.5, Cr.7, Cr. 8 , Cr.13, Cr.15, AT-1907) relying on a model that has been previously developed for the study of fossil hominins (Martínez et al., 2004, 2013; Quam et al., 2015, 2017). Sound power transmission through the outer and middle ear is strongly correlated with auditory sensitivity up to at least 5 kHz, and this approach accurately predicted the auditory capacities in humans and chimpanzees and has also been applied to fossil hominin individuals (Martínez et al., 2004, 2013; Quam et al., 2015, 2017). Relying on this method, we have established the pattern of sound power transmission through the right and left outer and middle ears in SH Cr.4 to evaluate the degree of CHL in this individual.

This method for estimating the sound power transmission relies on modeling the EAC as a cylinder. Since the EAC in SH Cr.4 has been altered by the presence of external auditory exostoses, it was necessary to modify the cylindrical model of the EAC to account for its peculiar form in SH Cr.4. To understand the influence of the external auditory exostoses on the hearing abilities in this individual, we have also reconstructed a theoretical non-pathological version of SH Cr.4 based on comparative measurements from other normal specimens in the SH sample. Finally, the results of both the pathological and non-pathological versions of the SH Cr.4 individual were compared with seven additional non-pathological individuals from the same site to see whether the hearing pattern(s) in SH Cr.4 differ from the rest of the sample. This represents a unique opportunity in paleontological research to compare a single, pathological individual with a sample of healthy individuals from the same biological population.

2. Materials and methods

The SH site is located in the Sierra de Atapuerca (Burgos, Spain) and has yielded the largest collection of Middle Pleistocene human fossils known (Arsuaga et al., 2014, 2015). From 1984 to 2018, more than 6900 human fossils have been recovered, corresponding to at least 28 individuals representing both females and males and ages of death between 11 and 50 years (Bermúdez de Castro et al., 2004; Bonmatí et al., 2010). The age of the SH site is firmly established at just over 430 ka by isotopic and biochronological methods (Arsuaga et al., 2014). For the comparative study of SH Cr.4, seven non-pathological individuals from the same site

have been used (Table 1). Since the EAC reaches adult size by the age of 9 years in modern humans (Wright, 1997), the inclusion of three adolescent individuals in the study is justified.

SH Cr.4 is one of the most complete crania from the SH site and was recovered during the 1992 field season (Arsuaga et al., 1993). This adult specimen preserves a complete neurocranium and is attributed to a male individual based on its generally large dimensions and brain size and the thickness of its cranial bones (Arsuaga et al., 1993, 1997, 2001). It preserves both right and left EAC, the right malleus (AT-5166) and the right (AT-6812) and left (AT-5499) incudes were also recovered from the tympanic cavities in this cranium.

2.1. CT scanning and 3D reconstruction

All the CT scanning was carried out with a YXLON Y.CT Compact scanner at the University of Burgos (Table 1). Virtual reconstructions and metric data collection were performed using Mimics© v.18 (Materialise, Leuven, Belgium) software following the standard procedure established in previous works (Martínez et al., 2004, 2013; Quam et al., 2015). The boundary between the temporal bone and the air-filled cavities has been established relying on the half maximum height thresholding protocol (Spoor et al., 1993; Spoor and Zonneveld, 1995; Coleman and Colbert, 2007) and was calculated as the average between the threshold for the EAC and that of the mastoid air cells. It is well-known that differences in spatial resolution of CT scans, as well as thresholding protocols can affect landmark placement and volumetric measurements in 3D reconstructions (Kim et al., 2012; Kubicka et al., 2016; Belgin et al., 2019). Nevertheless, the volume measurements included in the model have a very low influence on the final results, and large errors (>50% difference) in measurement would be necessary to alter the sound power transmission results in the SH crania (Supplementary Online Material [SOM] Text S1; SOM Table S1).

Most of the measures necessary for estimating the sound power transmission were taken on the 3D models using Mimics© (Fig. 1; Table 2). These measurements are physiologically relevant for hearing, and include measurements, the volumes of the tympanic cavity and mastoid air cells (Fig. 1a), size of the EAC (Fig. 1b,c), the tympanic membrane (Fig. 1c) and the aditus (Fig. 1d), and some measurements of the ear ossicles (Fig. 1d). However, the areas of the entry and exit of the aditus ($A_{AD(entrance)}$ and $A_{AD(exit)}$; Table 2; Fig. 1d) and the

151 area of the cross-section of the EAC (A_{EAC}; Table 2; Fig. 1c) were measured in 2D images with
152 Photoshop© CS5.
153
154 *2.2. Reconstruction of the EAC in SH Cr.4*
155 The EAC is comprised of two anatomical structures. On the one hand, the bony external
156 auditory canal (bony EAC), or meatus acusticus externus osseus (Gray, 1913), is formed by the
157 squamous portion of the temporal bone in its upper half and by the tympanic bone in its lower
158 half. Lateral to the bony EAC is the cartilaginous external auditory canal (cartilaginous EAC), or
159 meatus acusticus externus cartilagineus (Gray, 1913). Both structures are responsible for
160 transmitting sounds from the outside environment to the tympanic membrane. Since only the bony
161 EAC is preserved in fossils, it is necessary to reconstruct the cartilaginous EAC dimensions (i.e.,
162 length and cross-sectional area) from the bony EAC measurements to study the transmission of
163 sound through the outer ear in fossil specimens (Table 2).
164 The length of the bony EAC (L_{bEAC}; Fig.1b; Table 2) is measured from the most
165 posterosuperior point of the tympanic groove medially to the most anterior point of the
166 suprameatal spine laterally. To estimate the total length of the EAC ($L_{EACcomplete}$; Table 2),
167 including the bony and cartilaginous portions, the length of the bony portion (LbEAC) is multiplied
168 by 1.5 following Masali et al. (1991). The cross-sectional area of the EAC (A_{EAC}; Table 2) is
169 constant, resembling a cylinder whose cross-sectional area can be measured at the
170 posterosuperior point of the insertion of the tympanic membrane (Martínez et al., 2004; Fig. 2;
171 Table 2).
172 In the case of SH Cr. 4, the exostosis has affected the bony EAC cross-section in the
173 posterosuperior region, at the insertion site of the tympanic membrane, in both ears (Fig. 3),
174 causing a partial stenosis that reduces the A_{EAC} value. Given this situation, we have chosen to
175 use the mean value for A_{EAC} based on seven healthy individuals from the SH site (A_{EAC}-SH = 39.4
176 mm^2) as the most prudent approach to the original value of A_{EAC} for SH Cr.4.
177 As mentioned previously, in a non-pathological individual the value of the bony A_{EAC}
178 is equivalent to the value of the cartilaginous A_{EAC}, but in the case of SH Cr.4 it is necessary to
179 establish to what extent the exostosis affected the cross-sectional area (CSA) along the length
180 of the bony EAC. In this perspective, we compare the CSA in CT slices of the bony EAC in SH

Cr.4 measured every 0.2 mm with the A_{EAC}-SH. When CSA is less than A_{EAC}-SH (i.e., CSA < A_{EAC}-SH), that section can be considered to be affected by the pathology and the CSA value of that section will be used as the real value for the A_{EAC}. In those regions in which the CSA values are greater than, or equal to, A_{EAC}-SH (i.e., CSA ≥ A_{EAC}-SH), they will be considered unaffected by the pathology and the value of A_{EAC}-SH will be used as real A_{EAC} values. In this way, it is possible to reconstruct the cross-sectional area of the cartilaginous EAC value of each section along the length of the bony EAC.

2.3. Estimating the sound power transmission in SH Cr.4

To calculate the sound power transmission in SH Cr.4, we followed the procedure described in Martínez et al. (2004; 2013) and Quam et al. (2015; see SOM Text S2), where the auditory structures are modeled as simple geometric bodies in which the sound power transmission is known. The EAC can be modeled as a cylinder, the concha as a horn, and the tympanic membrane as a thin membrane. The circuit analogy of these simple geometric structures, such as a tube and a horn, is a two-port network, known as a quadripole. The auditory system of the outer and middle ear is then modeled as a cascade of two-port networks from the lateral edge of the external ear canal to the cochlea, in which the transmission value of the entire set is equal to the product of the transmission of each of the two-port networks included in the model (Rosowski, 1991, 1996; Quam et al., 2015).

The EAC has a strong influence on the sound power transmission results (Martínez et al., 2004; SOM Table S1), so its modeling is especially important in the establishment of the sound power transmission in SH Cr.4. To ensure the reliability of our results, we provide an analysis of the intraobserver and interobserver measurement error and the effects on the sound power transmission curves in the SOM (SOM Text S3; SOM Tables S2 and S3; SOM Figs. S1 and S2). Typically, the cartilaginous EAC is modeled as a cylinder whose length is $L_{EACcomplete}$ and the cross-sectional area is A_{EAC} (Fig. 2; Table 2). However, in SH Cr. 4, 2D CT images of several cuts along the length of the canal show that the respective sections are clearly deformed (Fig. 4), and therefore the simple cylinder model does not reflect its true form.

The non-pathological region of the EAC (CSA ≥ A_{EAC}-SH) can be modeled as a cylinder whose length corresponds to the length of the non-pathological segment of the EAC and whose

211 A_{EAC} corresponds to the mean value in the SH sample (A_{EAC}-SH). In the pathological region of
212 the EAC, it is necessary to establish the changes of form experienced by the EAC to determine
213 if the pathological region can still be modeled by one or more geometric bodies. With all this, the
214 EAC can be modeled as the married association of the quadrupole corresponding to the healthy
215 region (cylinder) and those corresponding to the different geometric bodies in which the
216 pathological region can be modeled.
217 To assess the effect of the pathology in SH Cr.4, the values of the sound power
218 transmission obtained are compared with those in a theoretically non-pathological SH Cr.4
219 individual. For this we have modeled its EAC as a cylinder of length $L_{EACcomplete}$ (Table 2) and
220 whose cross-sectional area is equal to A_{EAC}-SH. Similarly, the sound power transmission in the
221 pathological and theoretically non-pathological SH Cr.4 individuals were compared with the
222 sound power transmission results for the non-pathological SH individuals to see how both
223 versions of SH Cr.4 compare with the rest of the sample.
224
225 **Results**
226 Table 3 provides the values for the anatomical variables measured in SH Cr.4 and the
227 summary statistics for the non-pathological SH sample. Figure 5 shows the CSA values of SH
228 Cr.4 measured every 0.2 mm from the most posterosuperior point of the tympanic membrane
229 insertion in both ears. In the right ear, the region affected by the exostosis (CSA < A_{EAC}-SH)
230 extends 9.2 mm from the tympanic membrane, and two different segments are recognizable.
231 The first segment (C_{right} in Fig. 5) has a length of 4.4 mm and a fairly constant CSA. The lateral
232 endpoint of this segment was delimited at the point where the CSA is larger than the CSA value
233 measured in the first slice closest to the tympanic membrane. This segment can be modeled as
234 a cylinder with an A_{EAC} equal to the average CSA of all the slices in this segment (19.9 mm^2)
235 and a length of 4.4 mm (sector C_{right} in Fig. 6). A second segment has a length of 4.8 mm (H_{right}
236 in Fig. 5) extends laterally and the value of CSA increases continuously. The lateral endpoint of
237 this segment was delimited by the last slice where the CSA value falls below the A_{EAC}-SH. This
238 segment can be modeled as a horn whose length is 4.8 mm and whose entrance and exit areas
239 are 21.2 mm^2 and 38.3 mm^2, respectively (sector H_{right} in Fig. 6). The non-pathological third

segment (CSA ≥ A_{EAC}-SH) is modeled as a cylinder with a length of 19.7 mm and a cross-sectional area equal to A_{EAC}-SH (right non-pathological region in Fig. 6).

In the left ear, the region affected by exostosis (CSA < A_{EAC}-SH) has a length of 7.2 mm from the tympanic membrane, and two different segments are recognizable. The first segment (C_{left} in Fig. 5) has a length of 1.2 mm and a fairly constant CSA. The lateral endpoint of this segment was delimited at the point where the CSA is larger than the value measured in the first slice closest to the tympanic membrane. This segment can be modeled as a cylinder with an A_{EAC} equal to the average CSA of all the slices in this segment (21.5 mm^2) and a length of 1.2 mm (sector C_{left} in Fig. 6). A second segment has a length of 6.0 mm (H_{left} in Fig. 5) extends laterally and the value of CSA increases continuously. The lateral endpoint of this segment was delimited by the last slice where the CSA falls below A_{EAC}-SH. This segment can be modeled as a horn whose length is 6 mm and whose entrance and exit areas are 22.8 mm^2 and 37.8 mm^2, respectively (sector H_{left} in Fig. 6). The non-pathological third segment (CSA ≥ A_{EAC}-SH) is modeled as a cylinder with a length of 19.6 mm and an A_{EAC} equal to the mean value in the SH sample (left non-pathological region in Fig. 6).

For comparative purposes, the left and right EAC in SH Cr.4 have also been modeled as if they were healthy. Both EAC were modeled as cylinders whose cross-sectional areas are equal to A_{EAC}-SH (39.4 mm^2) and whose lengths correspond to the respective values for $L_{EACcomplete}$ (28.9 mm in the right ear and 26.8 mm in the left ear; Table 3). We then estimated the pattern of sound power transmission through the outer and middle ear between 0–5 kHz in both cartilaginous EAC (pathological and healthy) in the right and left ears of SH Cr.4 (Table 4; Fig.7). We have also modeled the sound power transmission in seven additional non-pathological individuals from the same site.

The sound power transmission values for SH Cr.4 in both pathological ears are close to the mean and within the range of variation in the non-pathological SH sample, over nearly the entire frequency range under study (Fig. 7; Table 4). Both pathological ears show a sound power transmission value slightly below the range of the other non-pathological SH individuals only at 5 kHz (0.7 dB in the right ear and 1.4 dB in the left ear). On the other hand, when comparing the sound power transmission values in SH Cr.4 for both the pathological and non-pathological reconstructions, no notable differences are observed. Only at 2 kHz does the right

ear, in which the region affected by the pathology is somewhat longer, show a slightly lower value (1.1 dB) of sound power transmission than in the normal reconstruction. Thus, it can be concluded that the exostoses did not significantly affect the hearing of the SH Cr.4 individual, neither when compared with the rest of SH sample nor when compared with the non-pathological version of itself.

Finally, the degree of stenosis of the EAC due to exostosis in SH Cr.4 has been quantified at the maximum point of occlusion of the EAC (i.e., minimum CSA), yielding values of 51.9% blockage in the right ear and 46.8% blockage in the left ear.

Discussion and conclusions

Auditory exostosis is a well-known pathology of the external ear in current clinical cases that is usually associated with a genetic predisposition (Steinbock, 1976; Hurst et al., 2004) or prolonged exposure to cold water (Kennedy, 1986; Wong et al., 1999; Wang et al., 2005; Cooper et al., 2010). In the case of SH Cr.4, given that similar pathologies are not found in the other SH individuals and that it is difficult to account for conditions that would imply a continuous exposure to cold water, Pérez et al. (1997) suggested that the most likely hypothesis for the origin of this pathology was an infectious process that stimulated an underlying genetic predisposition.

Several studies have classified the degree of stenosis of the EAC based on otoscopic inspection (Crowe et al., 2010; Attlmayr and Smith, 2015). Our results in SH Cr.4 allow us to classify the exostosis of both ears as grade 2 according to the classification of Crowe et al. (2010) and moderate stenosis according to that of Attlmayr and Smith (2015). Other cases of exostoses are known in the bony EAC of Pleistocene *Homo* fossils, including the Shanidar 1 Neandertal specimen and the Asian archaic *Homo* individuals Xuchang 1 and 2 and Xujiayao 15 (Trinkaus and Villotte, 2017; Trinkaus and Wu, 2017). Following the classification of Crowe et al. (2010), the authors have classified the exostoses of Xujiayao 15 and Xuchang 1 as grade 1 and grade 2, respectively, while Shanidar 1 and Xuchang 2 were considered as grade 3. Therefore, the exostosis present in the SH Cr.4 is more pronounced than that of Xujiayao 15, equivalent to that of Xuchang 1 and less pronounced than those of Shanidar 1 and Xuchang 2.

Most cases of exostosis are asymptomatic, and only when there is a severe stenosis of the EAC does one suffer hearing loss, recurrent external ear infections and a sense of ears being 'plugged' (Lennon et al., 2016). At the same time, in cases of EAC exostosis that are associated with conductive hearing loss, this is not usually caused by the stenosis itself, but, rather, is a consequence of the accumulation of detritus and wax that can cause external ear infections (Kennedy, 1986; Whitaker et al. al., 1998) and that can produce a hearing loss of up to 50 dB (Graham, 1979). These accumulations, and the associated infections, usually appear in clinical cases with a level of occlusion of the EAC which is greater than 80% and are very uncommon in patients with an occlusion of less than 60% (Whitaker et al., 1998). In SH Cr.4 the occlusion of the bony EAC is 51.9% in the right ear and 46.8% in the left ear, which makes it very unlikely that wax accumulations would occur leading to recurrent severe external ear infections that could cause important hearing losses. In summary, the results of our study indicate that the level of stenosis caused by the exostosis of both bony EAC of SH Cr.4 would not have produced an appreciable decrease in the sound power transmission through the outer and middle ear. At the same time, the level of stenosis of the bony EAC of SH Cr.4 is not severe enough to expect recurrent infections produced by the accumulation of wax and detritus. Therefore, it is reasonable to conclude that the SH Cr.4 individual did not suffer conductive hearing loss as a consequence of the exostosis in their EAC. This result can be extended to other fossils in which a degree of stenosis less than or equal to that of SH Cr.4 has been reported, such as the cases of Xujiayao 15 and Xuchang 1 (Trinkaus and Wu, 2017). In the cases of Shanidar 1 and Xuchang 2, with a degree of stenosis greater than that of SH Cr.4 (Trinkaus and Villotte, 2017; Trinkaus and Wu, 2017), the possibility remains that they suffered a loss of hearing as a result of the exostoses in their EAC. Virtual study of the EAC in these individuals, following similar procedures as those outlined here, would allow for confirmation of this suggestion.

References

Arsuaga, J.L., Martínez, I., Gracia, A., Carretero, J.M., Carbonell, E., 1993. Three new human skulls from the Sima de los Huesos Middle Pleistocene site in Sierra de Atapuerca, Spain. Nature 362, 534–537.

329 Arsuaga, J.L., Martínez, I., Gracia, A., Lorenzo, C., 1997. The Sima de los Huesos crania
330 (Sierra de Atapuerca, Spain). A comparative study. Journal of Human Evolution 33,
331 219–281.
332 Arsuaga, J.L., Martínez, I., Gracia, A., 2001. Analyse phylogénétique des Hominidés de la
333 Sierra de Atapuerca (Sima de los Huesos et Gran Dolina TD-6): L'évidence crânienne.
334 L'Anthropologie 105, 161–178.
335 Arsuaga, J.L., Carretero, J. M., Lorenzo, C., Gómez-Olivencia, A., Pablos, A., Rodríguez, L.,
336 García-González, R., Bonmatí, A., Quam, R., Pantoja-Pérez, A., Martínez, I., Aranburu,
337 A., Gracia-Téllez, A., Poza-Rey, E., Sala, N., García, N., Alcázar de Velasco, A.,
338 Cuenca-Bescós, G., Bermúdez de Castro, J.M., Carbonell, E., 2015. Postcranial
339 morphology of the middle Pleistocene humans from Sima de los Huesos, Spain.
340 Proceedings of the National Academy of Sciences USA 112, 11524-11529.
341 Arsuaga, J.L., Martínez, I., Arnold, L., Aranburu, A., Gracia-Téllez, A., Sharp, W., Quam, R.,
342 Falguères, C., Pantoja-Pérez, A., Bischoff, J., Poza-Rey, E., Parés, J., Carretero, J.,
343 Demuro, M., Lorenzo, C., Sala, N., Martinón-Torres, M., García, N., Alcázar de Velasco,
344 A., Cuenca-Bescós, G., Gómez-Olivencia, A., Moreno, D., Pablos, A., Shen, C.,
345 Rodríguez, L., Ortega, A., García, R., Bonmatí, A., Bermúdez de Castro, J.M.,
346 Carbonell, E., 2014. Neandertal roots: Cranial and chronological evidence from Sima de
347 los Huesos. Science 344, 1358-1363.
348 Attlmayr, B., Smith, I.M., 2015. Prevalence of "surfer´s ear" in Cornish surfers. The Journal of
349 Laryngology & Otology 129, 440-444.
350 Bermúdez de Castro, J. M., Martinon-Torres, M., Lozano, M., Sarmiento, S., Muela, A., 2004.
351 Paleodemography of the Atapuerca: Sima de los Huesos Hominin sample: A revision and
352 new approaches to the paleodemography of the European Middle Pleistocene population.
353 Journal of Anthropological Research 60, 5-26.
354 Belgin, C.A., Serinderea G., Orhan, K., 2019. Accuracy and reliability of enamel and dentin
355 thickness measurements on micro-computed tomography and digital periapical
356 radiographs. Journal of Forensic Radiology and Imaging.
357 https://doi.org/10.1016/j.jofri.2019.05.006.

Bonmatí, A., Gómez-Olivencia, A., Arsuaga, J.L., Carretero, J.M., Gracia, A., Martínez, I., Lorenzo, C., Bermúdez de Castro, J.M., Carbonell, E., 2010. Middle Pleistocene lower back and pelvis from an aged human individual from the Sima de los Huesos site, Spain. Proceedings of the National Academy of Sciences USA 107, 18386-18391.

Buikstra, J.E., 2010. Paleopathology: a contemporary perspective. In: Larson, C.S. (Ed.), Companion to Biological Anthropology. Wiley-Blackwell, Chichester, pp. 395-411.

Calderon, R., Greenberg, M., 2003. Social and emotional development of deaf children. In: Marschark, M., Spencer, P.E. (Eds.), Oxford Handbook of Deaf Studies, Language, and Education, Oxford University Press, New York, pp. 177-189.

Coleman, M.N., Colbert, M.W., 2007. Technical note: CT thresholding protocols for taking measurements on three-dimensional models. American Journal of Physical Anthropology 133, 723-725.

Cooper, A., Tong, R., Neil, R., Owens, D., Tomkinson, A., 2010. External auditory canal exostoses in white water kayakers. British Journal of Sports Medicine 44, 144-147.

Coqueugniot, H., Dutour, O., Arensburg, B., Duday, H., Vandermeersch, B., Tillier, A.M., 2014. Earliest cranio-encephalic trauma from the Levantine Middle Palaeolithic: 3D reappraisal of the Qafzeh 11 skull, consequences of pediatric brain damage on individual life condition and social care. PLoS One 9, e102822.

Crowe, F., Sperduti, A., O'Connell, T. C., Craig, O. E., Kirsanow, K., Germoni, P., Macchiarelli, R., Garnsey, P., Bondioli, L., 2010. Water-related occupations and diet in two Roman coastal communities (Italy, first to third century AD): Correlation between stable carbon and nitrogen isotope values and auricular exostosis prevalence. American Journal of Physical Anthropology 142, 355-366.

Gracia, A., Arsuaga, J.L., Martínez, I., Lorenzo, C., Carretero, J.M., Bermúdez de Castro, J.M., Carbonell, E., 2009. Craniosynostosis in the Middle Pleistocene human Cranium 14 from the Sima de los Huesos, Atapuerca, Spain. Proceedings of the National Academy of Sciences USA 106, 6573-6578.

Gracia, A., Martínez-Lage, J.F., Arsuaga, J.L., Martínez, I., Lorenzo, C., Pérez-Espejo, M.A., 2010. The earliest evidence of true lambdoid craniosynostosis: the case of “Benjamina”, a *Homo heidelbergensis* child. Child’s Nervous System 26, 723-727.

Gracia, A., Arsuaga, J.L., Martínez, I., Martín-Francés, L., Martinón-Torres, M., Bermúdez de Castro, J.M., Bonmatí, A., Lira, J., 2012. Orofacial pathology in *Homo heidelbergensis*: The case of Skull 5 from the Sima de los Huesos site (Atapuerca, Spain). Quaternary International 295, 83-93.

Graham, M.D., 1979. Osteomas and exostoses of the external auditory canal: A clinical, histopathologic and scanning electron microscopic study. Annals of Otology, Rhinology and Laryngology 88, 566-572.

Gray, H., 1913. Anatomy Descriptive and Applied. Lea & Febiger, Philadelphia and New York

Hurst, W., Bailey, M., Hurst, B., 2004. Prevalence of external auditory canal exostoses in Australian surfboard riders. The Journal of Laryngology & Otology 118, 348-351.

Kennedy, G.E., 1986. The relationship between auditory exostoses and cold water: a latitudinal analysis. American Journal of Physical Anthropology 71, 401-415.

Kim, G., Jung, H.J., Lee, H.J., Lee, J.S., Koo, S., Chang, S.H., 2012. Accuracy and reliability of length measurements on three-dimensional computed tomography using open-source OsiriX software, Journal of Digital Imaging 25, 486-491.

Kubicka, A.M., Stefaniak, J., Lubiatowski, P., Długosz, J., Dzianach, M., Redman, M., Piontek, J., Romanowski, L., 2016. Reliability of measurements performed on two dimensional and three dimensional computed tomography in glenoid assessment for instability. International Orthopaedics 40, 2581-2588.

Lennon, P., Murphy, C., Fennessy, B., Hughes, J.P., 2016. Auditory canal exostoses in Irish surfers. Irish Journal of Medical Science 185, 183-187.

Lovell, N.C., 1997. Trauma analysis in paleopathology. American Journal of Physical Anthropology 104, 139-170.

Martínez, I., Rosa, M., Arsuaga, J.L., Jarabo, P., Quam, R., Lorenzo, C., Gracia, A., Carretero, J.M., Bermúdez de Castro, J.M., Carbonell, E., 2004. Auditory capacities in Middle Pleistocene humans from the Sierra de Atapuerca in Spain. Proceedings of the National Academy of Sciences USA 101, 9976-9981.

Martínez, I., Rosa, M., Quam, R., Jarabo, P., Lorenzo, C., Bonmatí, A., Gómez-Olivencia, A., Gracia, A., Arsuaga, J.L., 2013. Communicative capacities in Middle Pleistocene humans from the Sierra de Atapuerca in Spain. Quaternary International 295, 94-101.

418 Masali, M., Maffei, M., Borgognini Tarli, S., 1991. Application of a morphometric model for the
419 reconstruction of some functional characteristics of the external and middle ear in Circeo
420 1. In: Piperno, M., Scichilone, G. (Eds.), The Circeo 1 Neandertal Skull: Studies and
421 Documentation. Instituto Poligrafico e Zecca Dello Stato, Rome, pp. 321-338.
422 Michaels, L., 2006. Ear and temporal bone. In: Cardesa, A., Slootweg, P.J. (Eds.), Pathology of
423 the Head and Neck. Springer Verlag, Berlin, pp. 234-260.
424 Pérez, P.J., Gracia, A., Martínez, I., Arsuaga, J.L., 1997. Paleopathological evidence of the cranial
425 remains from the Sima de los Huesos Middle Pleistocene site (Sierra de Atapuerca,
426 Spain). Description and preliminary inferences. Journal of Human Evolution 33, 409-421.
427 Quam, R., Martínez, I., Rosa, M., Bonmatí, A., Lorenzo, C., de Ruiter, D.J., Moggi-Cecchi, J.,
428 Conde-Valverde, M., Jarabo, P., Menter, C.G., Thackeray, J.F., Arsuaga, J.L., 2015.
429 Early hominin auditory capacities. Science Advances 1, e1500355.
430 Quam, R., Martínez, I., Rosa, M., Arsuaga, J.L., 2017. Evolution of hearing and language in fossil
431 hominins. In: Quam, R., Ramsier, M.A., Fay, R., Popper, A. (Eds.), Primate Hearing and
432 Communication. Springer International, Cham, pp. 201-231.
433 Rhys-Evans, P.H., Cameron, M., 2017. Aural exostoses (surfer's ear) provide vital fossil evidence
434 of an aquatic phase in Man's early evolution. The Annals of the Royal College of
435 Surgeons of England 99, 594-601.
436 Rosowski, J., 1991. The effects of external and middle ear filtering on auditory threshold and
437 noise-induced hearing loss. The Journal of the Acoustical Society of America 90, 124-
438 135.
439 Rosowski, J., 1996. Models of external and middle-ear function. In: Hawkins, H., McMullen, T.,
440 Popper, A., Fay, R. (Eds.), Auditory Computation, Springer, New York, pp. 15-61.
441 Sala, N., Arsuaga, J.L., Pantoja-Pérez, A., Pablos, A., Martínez, I., Quam, R.M., Gómez-
442 Olivencia, A., Bermúdez de Castro, J.M., Carbonell, E., 2015. Lethal interpersonal
443 violence in the Middle Pleistocene. PLoS One 10, e0126589.
444 Sheehy, J.L., 1958. Osteoma of the external auditory canal. The Laryngoscope 68, 1667-1673.
445 Steinbock, R.T., 1976. Paleopathological diagnosis and interpretation: bone diseases in ancient
446 human populations. Charles C Thomas Pub Limited, Springfield.

447 Stevenson, J., McCann, D., Watkin, P., Worsfold, S., Kennedy, C., 2010. The relationship
448 between language development and behaviour problems in children with hearing loss.
449 Journal of Child Psychology and Psychiatry 51, 77-83.
450 Spoor, F., Zonneveld, F., 1995. Morphometry of the primate bony labyrinth: a new method based
451 on high-resolution computed tomography. Journal of Anatomy 186, 271-286.
452 Spoor, F., Zonneveld, F., Macho, G.A., 1993. Linear measurements of cortical bone and dental
453 enamel by computed tomography: applications and problems. American Journal of
454 Physical Anthropology 91, 469-484.
455 Tilley, L., Oxenham, M.F., 2011. Survival against the odds: Modeling the social implications of
456 care provision to seriously disabled individuals. International Journal of Paleopathology
457 1, 35-42.
458 Trinkaus, E., Villotte, S., 2017. External auditory exostoses and hearing loss in the Shanidar 1
459 Neandertal. PLoS One 12, e0186684.
460 Trinkaus, E., Wu, X.J., 2017. External auditory exostoses in the Xuchang and Xujiayao human
461 remains: Patterns and implications among eastern Eurasian Middle and Late Pleistocene
462 crania. PLoS One 12, e0189390.
463 Walling, A.D., Dickson, G.M., 2012. Hearing loss in older adults. American Family Physician 85,
464 1150-1156.
465 Wang, M.C., Liu, C.Y., Shiao, A.S., Wang, T., 2005. Ear problems in swimmers. Journal of the
466 Chinese Medical Association 68, 347-352.
467 Whitaker, S.R., Cordier, A., Kosjakov, S., Charbonneau, R., 1998. Treatment of external auditory
468 canal exostoses. The Laryngoscope 108, 195-199.
469 Wilbur, A.K., Farnbach, A.W., Knudson, K.J., Buikstra, J.E., 2008. Diet, tuberculosis, and the
470 paleopathological record. Current Anthropology 49, 963-991.
471 Wright, C.G., 1997. Development of the human external ear. Journal American Academy of
472 Audiology 8, 379-382.
473 Wong, B.J., Cervantes, W., Doyle, K.J., Karamzadeh, A.M., Boys, P., Brauel, G., Mushtaq, E.,
474 1999. Prevalence of external auditory canal exostoses in surfers. Archives of
475 Otolaryngology–Head & Neck Surgery 125, 969-972.
476

FIGURE CAPTIONS

Figure 1. 3D model of the temporal bone SH Cr.7 (AT-804) showing the definitions of the anatomical variables used to estimate the sound power transmission through the outer and middle ear. a) Complete 3D model of the ear structures. b) 3D model of the temporal bone and external auditory canal (EAC) showing the measurement of the length of the bony EAC. c) 3D model of the EAC showing measurement of the size of the tympanic membrane and cross-section of the EAC. d) 3D model of the aditus ad antrum showing definition of the aditus entrance and exit measurements. e) Measurements of the auditory ossicles. Abbreviations: V_{MA} = volume of mastoids cells; V_{MEC} = volume of the middle ear cavity; L_{bEAC} = length of the bony EAC; R_{TM1} = half of the greater diameter of the tympanic membrane; R_{TM2} = half of the lesser diameter of the tympanic membrane; A_{EAC} = area of the cross-section of the EAC; $A_{AD(exit)}$ = area of the exit of the aditus to the mastoid antrum; $A_{AD(entrance)}$ = area of the entrance to the aditus from the middle ear cavity; L_{AD} = length of the aditus: L_M = functional length of the malleus; L_I = functional length of the incus; A_{FP} = area of the stapes footplate. See Table 2 for measurement definitions.

Figure 2. Coronal slice of the temporal bone of SH Cr.7 (AT-804) showing the cylindrical model of a non-pathological external auditory canal (EAC): A = plane of the tympanic membrane; B = axis of the EAC from the center of the tympanic membrane to the center of the external acoustic meatus. In normal ears, the cartilaginous EAC is typically modeled as a cylinder and extends laterally beyond the bony EAC. White arrow = posterosuperior point of the insertion of the tympanic membrane. Complete length of the EAC ($L_{EACcomplete}$) and the cross-sectional area of the EAC (A_{EAC}) as defined in Table 2. Abbreviations: L = left side; R = right side. Scale bar = 5 mm.

Figure 3. Comparison of the CT images showing the cross-sectional area of the bony EAC at the posterosuperior insertion point of the tympanic membrane (A_{EAC}) in a non-pathological, normal individual (a) and that in SH Cr.4 (b, c) showing stenosis: a) SH Cr.7; b) SH Cr.4, left; c) SH Cr.4, right. Scale bar = 1 mm.

Figure 4. 3D reconstruction of the outer and middle ear structures in the right ear of SH Cr.4 showing the mastoid air cells (purple), aditus ad antrum (green), tympanic cavity (yellow), Eustachian tube (pink) and EAC (blue). Three slices along the length of the EAC (insets 1, 2, 3)

show the variation in the cross-section. Point 1 corresponds to the posterosuperior insertion of the tympanic membrane. Point 2 is placed 4.4 mm lateral of Point 1. Point 3 is placed 4.8 mm lateral of Point 2, and represents the lateral limit of the pathological section of the EAC. Scale bars = 5 mm (main figure) and 1 mm (insets).

Figure 5. Cross-sectional area (CSA) of the pathological segment of the bony external auditory canal (EAC) in SH Cr.4. CT Slices are separated by 0.2 mm starting from the most posterosuperior point of the tympanic membrane insertion. The values of the left ear (triangles) and the right ear (circles) are represented. The dashed line represents the mean area of the EAC (A_{EAC}) value for the non-pathological SH sample (i.e., A_{EAC}-SH).All sections below that line are affected by exostosis and all sections above that line are considered non-pathological. The C_{left} and C_{right} regions correspond to those sections whose CSA is approximately constant and are modeled as a cylinder. The H_{left} and H_{right} regions correspond to those sections whose CSA values increase continuously with distance from the tympanic membrane and are modeled as a horn.

Figure 6. Graphic representation of the model of the external auditory canal (EAC) in both ears of SH Cr.4 based on simple geometric shapes. Abbreviations: C_R = right segment modeled as a cylinder; H_R = right segment modeled as a horn; C_L = left segment modeled as a cylinder; H_L = left segment modeled as a horn.

Figure 7. Graphic representation of the pattern of sound power transmission in both ears (pathological and normal) of SH Cr.4 and in seven additional non-pathological individuals from the same site. P_0 is a threshold value of sound power, equal to 10^{-18} W. $P_{cochlea}$ refers to the sound power at the entrance to the cochlea for an incident plane wave intensity of 10^{-12} W/m^2.

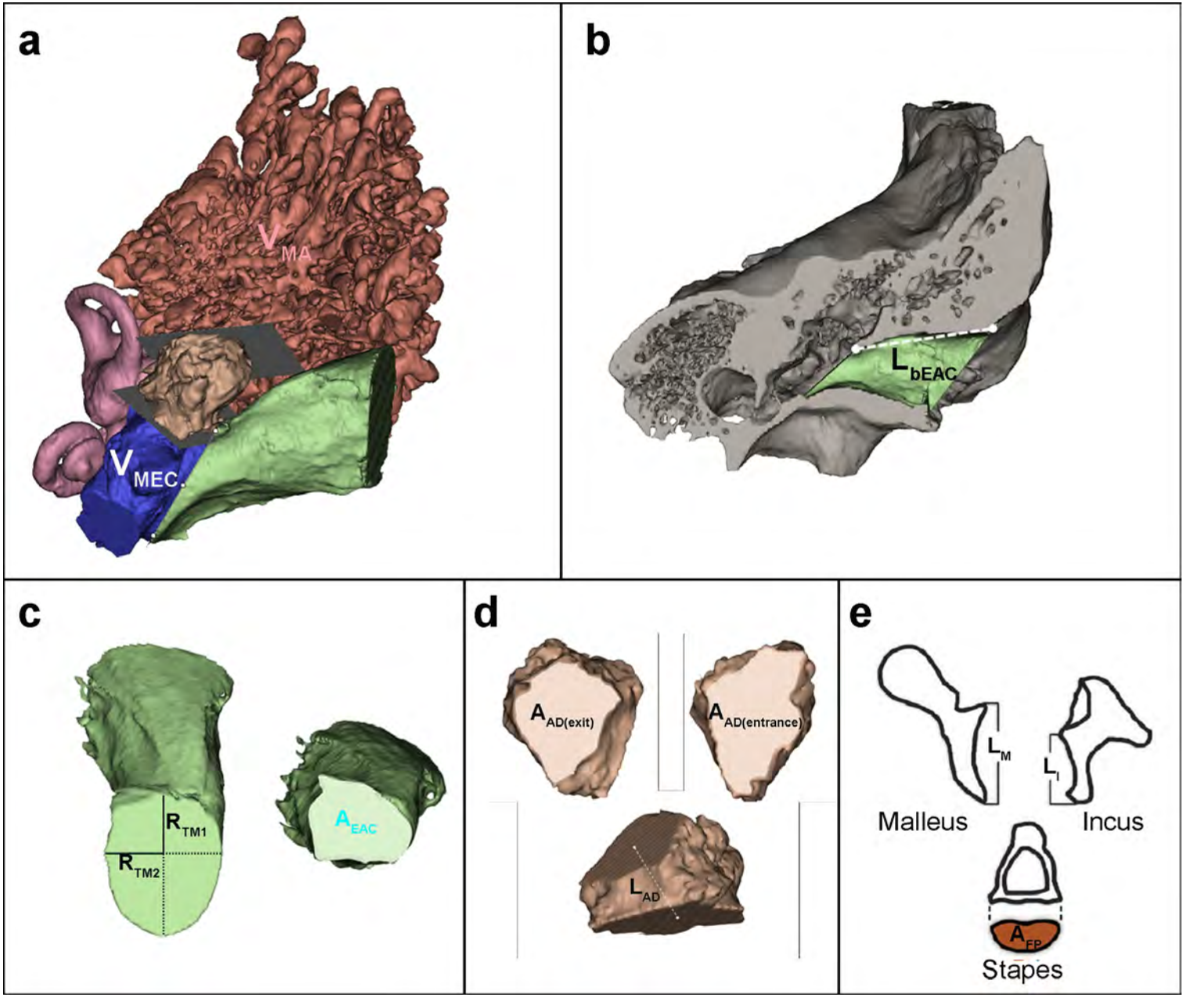
a
V_{MA}
V_{MEC}
b
L_{bEAC}
c
R_{TM1}
R_{TM2}
A_{EAC}
d
$A_{AD(exit)}$
$A_{AD(entrance)}$
L_{AD}
e
L_M
L_I
Malleus
Incus
A_{FP}
Stapes

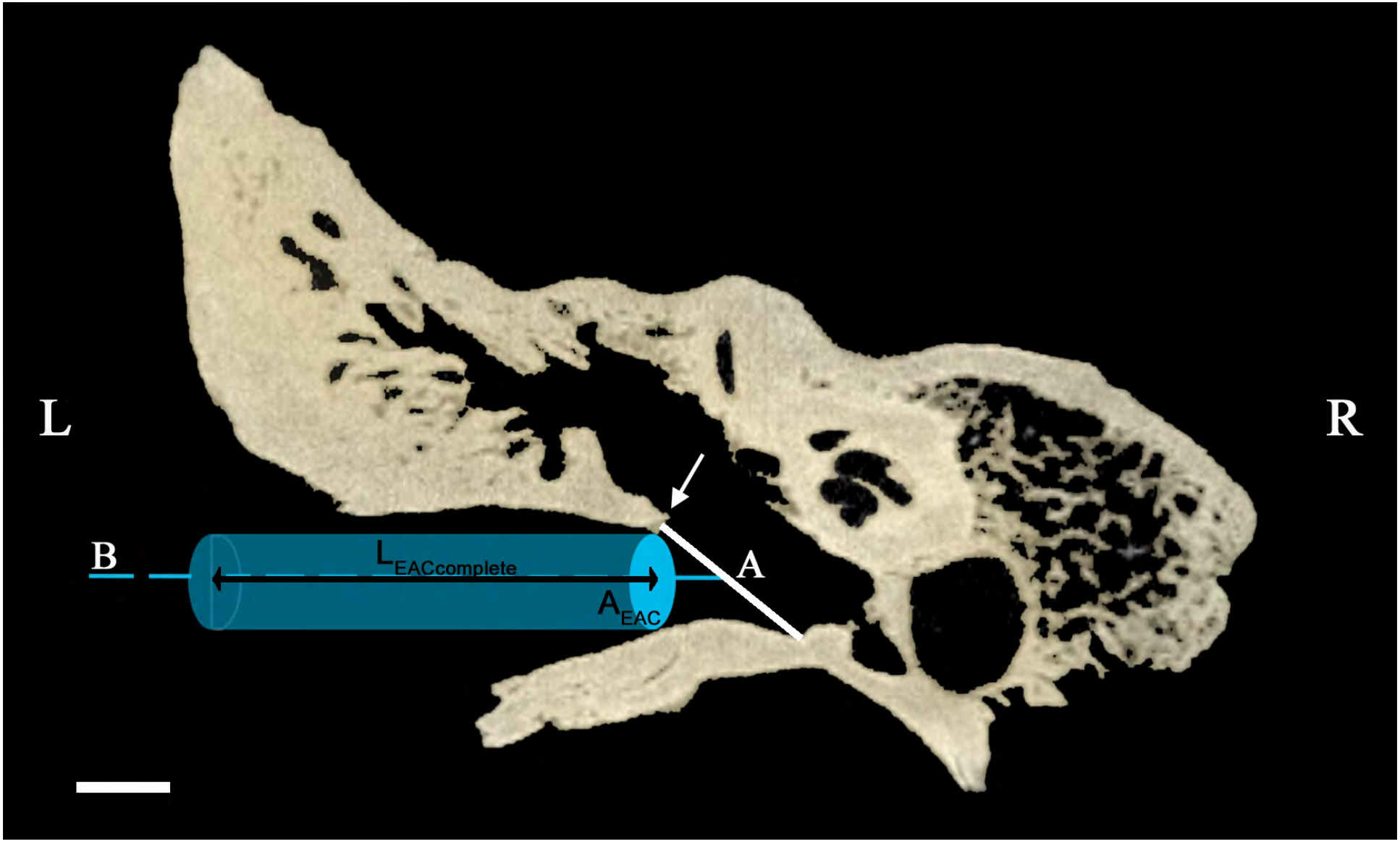
L
R
B
A
$L_{EACcomplete}$
A_{EAC}

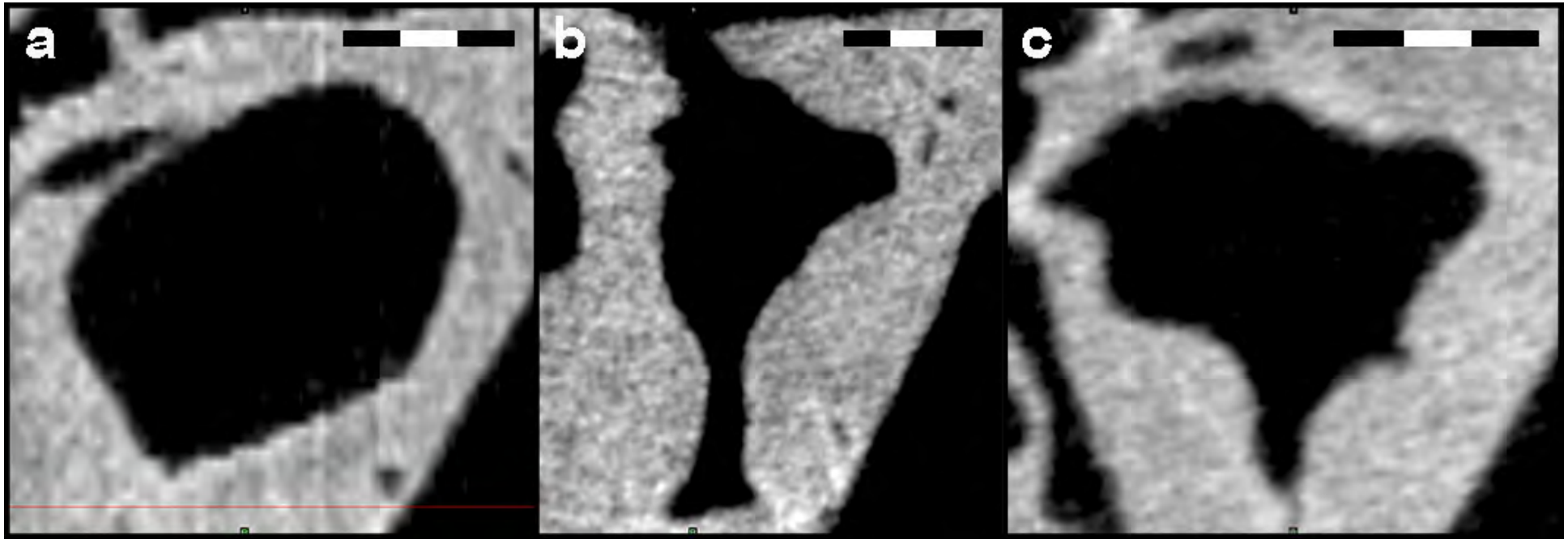
a
b
c

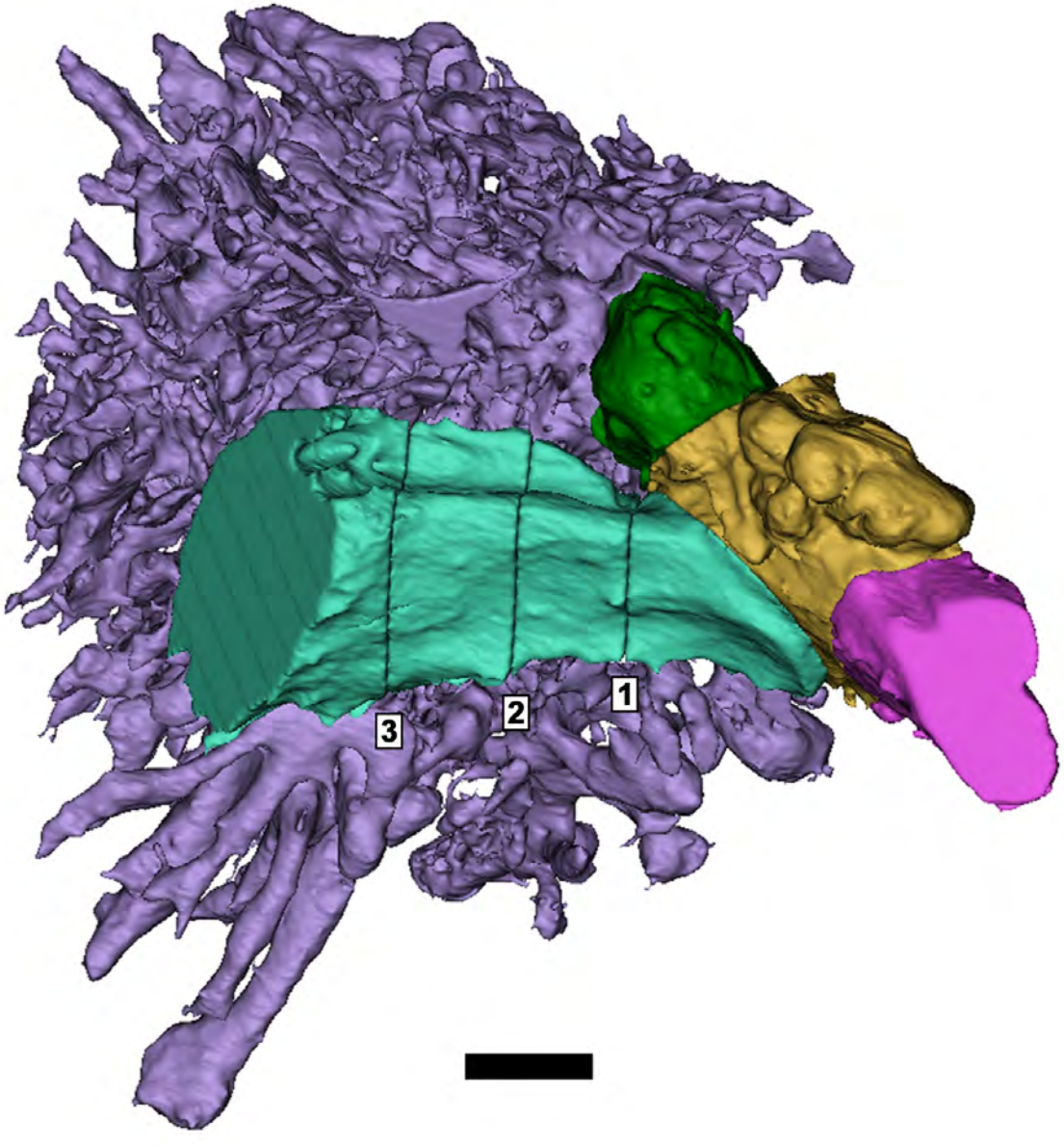
1
2
3

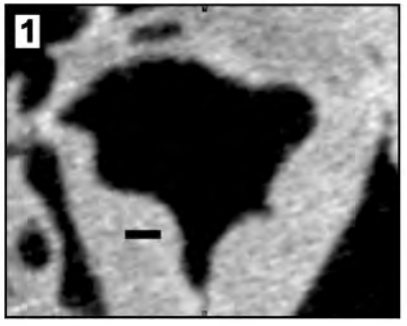
1


2

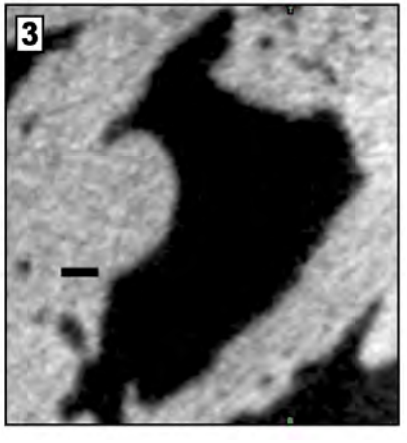
3

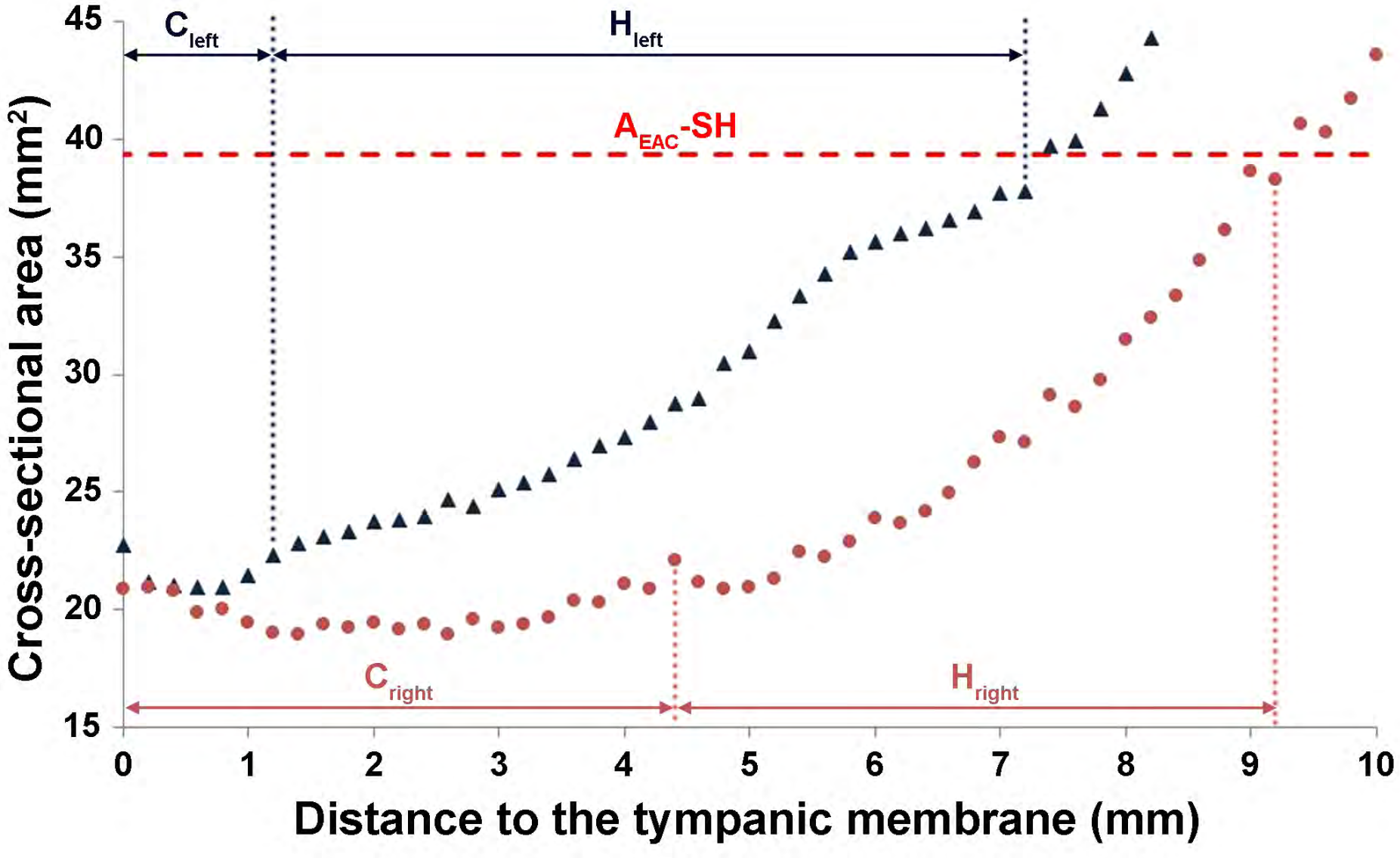
C left
H left
A EAC-SH
C right
H right
Cross-sectional area (mm²)
Distance to the tympanic membrane (mm)
45
40
35
30
25
20
15
0
1
2
3
4
5
6
7
8
9
10

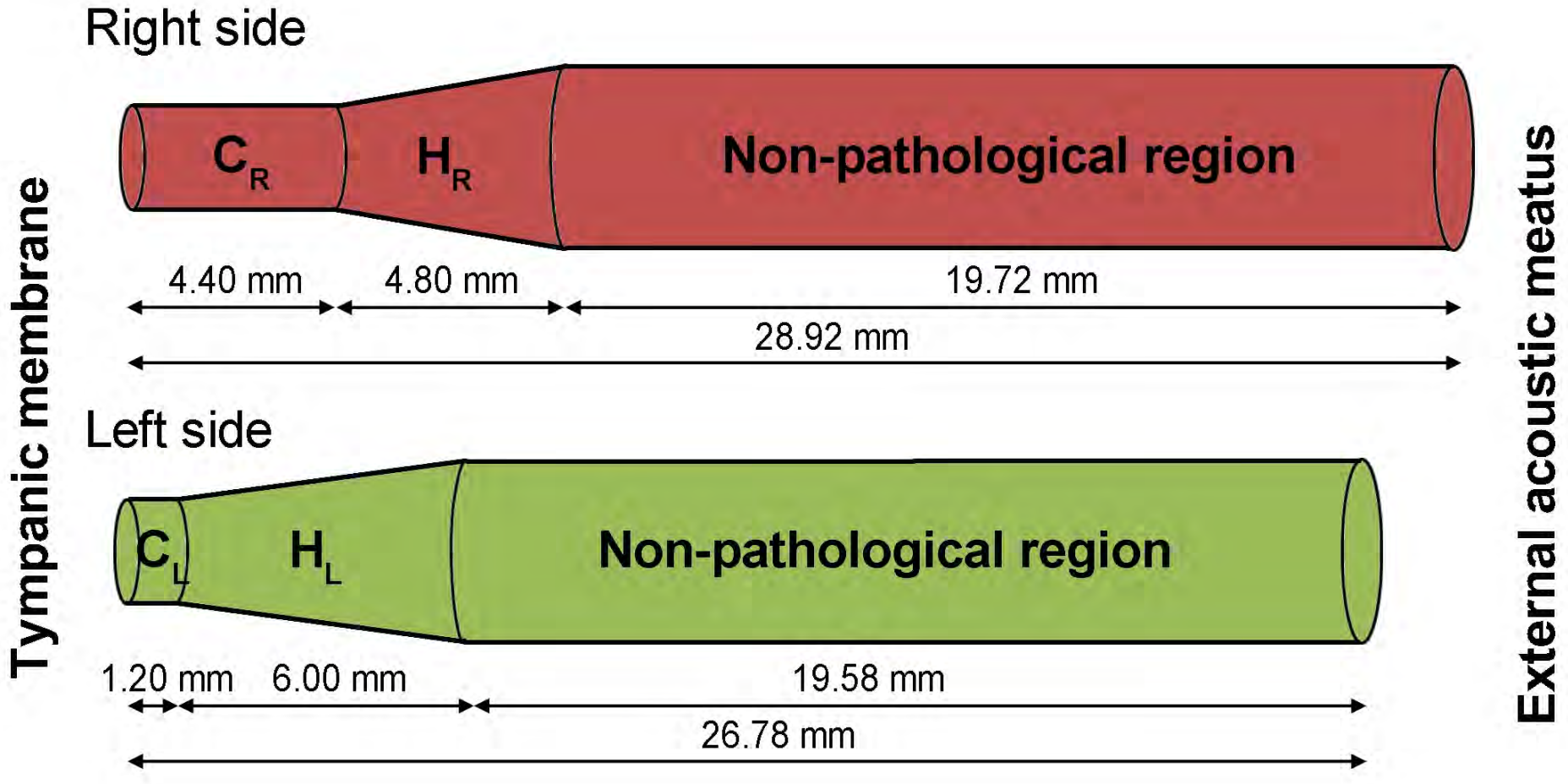
Right side
C_R
H_R
Non-pathological region
4.40 mm
4.80 mm
19.72 mm
28.92 mm
Left side
C_L
H_L
Non-pathological region
1.20 mm
6.00 mm
19.58 mm
26.78 mm
Tympanic membrane
External acoustic meatus

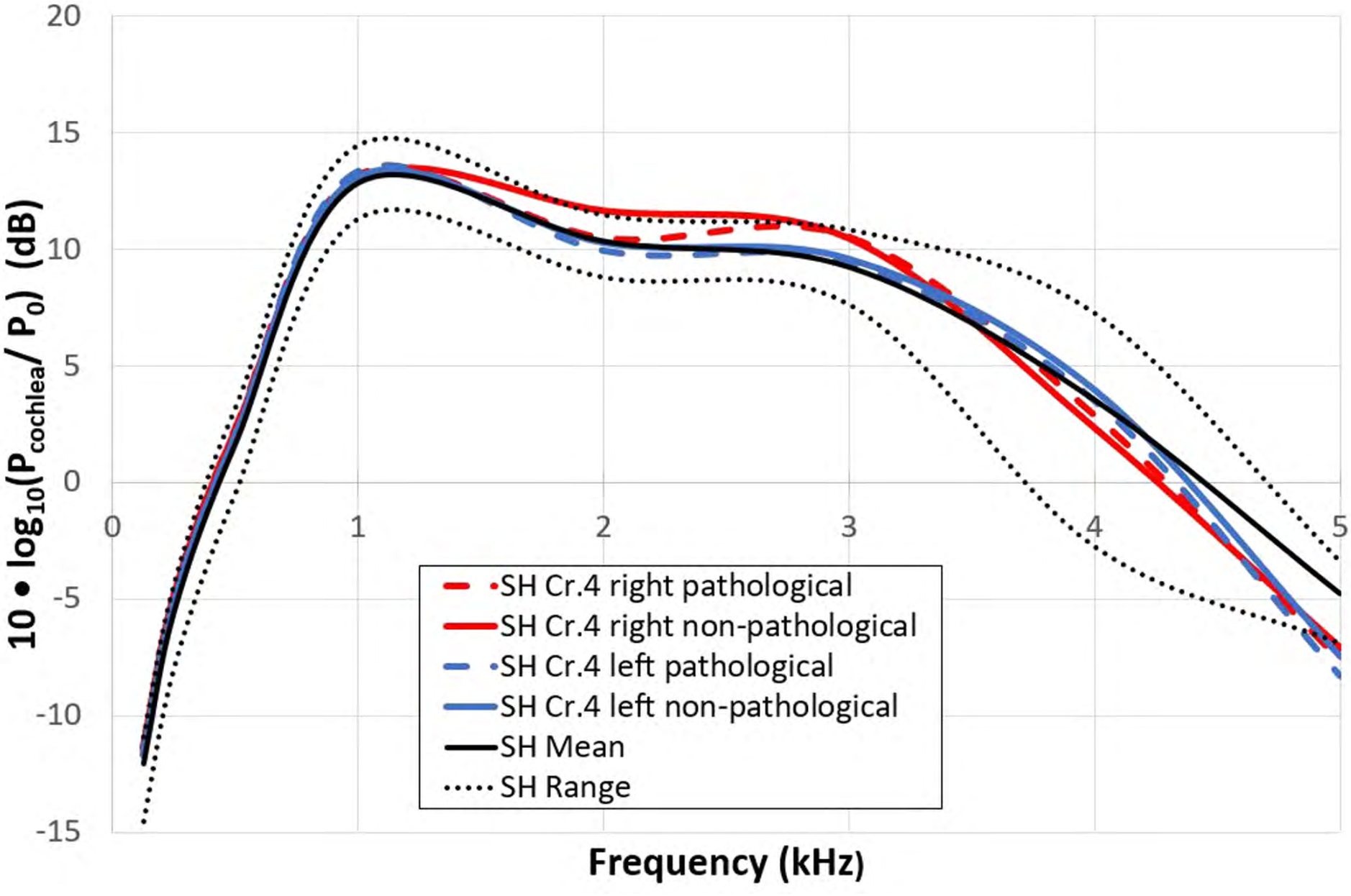
20
15
10
5
0
-5
-10
-15
0
1
2
3
4
5
10 • log10(Pcochlea/ P0) (dB)
Frequency (kHz)
SH Cr.4 right pathological
SH Cr.4 right non-pathological
SH Cr.4 left pathological
SH Cr.4 left non-pathological
SH Mean
SH Range

Table 1

SH sample and CT scanning parameters.

Specimen	Side	Age at death	Number of slices	Slice increment (mm)	Pixel size (mm)	Image size (pixels)	Field of view (mm)	Voltage (kV)	Current (mA)
Cr.3	Left	Adolescent	303	0.2	0.033	2048	67.53	160.00	4.00
Cr.4	Right	Adult	332	0.2	0.033	2048	67.53	160.00	4.00
Cr.4	Left	Adult	307	0.2	0.033	2048	67.53	160.00	4.00
Cr.5	Left	Adult	330	0.2	0.029	2048	59.91	170.00	3.75
Cr.7	Left	Adolescent	230	0.2	0.073	2048	149.9	170.00	3.75
Cr.8	Left	Adult	285	0.2	0.035	2048	71.21	160.00	4.00
Cr.13	Right	Adult	347	0.2	0.033	2048	67.53	170.00	3.75
Cr.15	Right	Adult	351	0.2	0.033	2048	67.53	160.00	4.00
AT-1907	Right	Adolescent	260	0.2	0.037	2048	75.01	160.00	4.00

Table 2

Measurements used to calculate the sound power transmission through the outer and middle ears.[a]

Measurement (unit)	Definition	Figure
V_{MEC} (mm^3)	Volume of the middle ear cavity, limited by the plane that coincides with the tympanic sulcus and by the entrance plane to the aditus ad antrum	Fig. 1a
V_{MA} (mm^3)	Combined volume of the mastoid antrum and the mastoid air cells connected to it	Fig. 1a
L_{bEAC} (mm)	Length of the bony external auditory canal measured from the most posterosuperior point of the tympanic sulcus to the most anterior point of the spina suprameatum	Fig. 1b
$L_{EACcomplete}$ (mm)	Length of the complete cartilaginous external auditory canal (EAC). To include the exclusively cartilaginous lateral portion of the EAC we have calculated it by multiplying the length of the bony EAC by a factor of 1.5, following Masali et al. (1991)	
A_{EAC} (mm^2)	Area of the cross-section of the EAC. Measured at the most posterosuperior point of the tympanic sulcus and perpendicular to the axis between the central point of the tympanic membrane and the central point of the external acoustic meatus	Fig. 1c
R_{TM1} (mm)	Half of the greater diameter of the tympanic membrane, measured in the tympanic sulcus	Fig. 1c
R_{TM2} (mm)	Half the lesser diameter of the tympanic membrane, measured in the tympanic sulcus perpendicular to the RTM1	Fig. 1c
A_{TM} (mm^2)	Tympanic membrane area calculated as an ellipse of radii RTM1 and RTM2	
$A_{AD(entrance)}$ (mm^2)	Area of the entrance to the aditus ad antrum entrance from the middle ear cavity	Fig. 1d

$A_{AD(exit)}$ (mm^2)	Area of the exit of the aditus ad antrum to the mastoid antrum	Fig. 1d
L_{AD} (mm)	Length of aditus ad antrum. Measured from the central point of the aditus ad antrum entrance to the central point of the aditus ad antrum exit.	Fig. 1d
$M_M + M_I$ (mg)	Combined mass of the malleus and incus	
L_M (mm)	Functional length of the malleus measured as the maximum length between the tip of the lateral process and the tip of the manubrium.	Fig. 1e
L_I (mm)	Functional length of the incus, measured as the length between the most anteroinferior point of the articular facet and the tip of the long process with the bone oriented in the axis of rotation	Fig. 1e
L_M/L_I	Ratio between the functional lengths of the malleus and the incus (middle ear lever ratio).	
M_S (mg)	Mass of the stapes	
A_{FP} (mm^2)	Area of the stapes footplate	Fig. 1e

Abbreviations: ; V_{MEC} = volume of the middle ear cavity; V_{MA} = volume of mastoids cells; L_{bEAC} = length of the bony EAC; $L_{EACcomplete}$ = complete length of the EAC; A_{EAC} = area of the cross-section of the EAC; R_{TM1} = half of the greater diameter of the tympanic membrane; R_{TM2} = half of the lesser diameter of the tympanic membrane; A_{TM} = area of the tympanic membrane; $A_{AD(entrance)}$ = area of the entrance to the aditus from the middle ear cavity; $A_{AD(exit)}$ = area of the exit of the aditus to the mastoid antrum; L_{AD} = length of the aditus; M_M = mass of the malleus; M_I = mass of the incus; L_M = functional length of the malleus; L_I = functional length of the incus; M_S = mass of the stapes; A_{FP} = area of the stapes footplate.

[a] Previously published in Martínez et al. (2004, 2013) and Quam et al. (2015).

Table 3

Measurements used in the estimation of the sound power transmission for SH Cr.4 and the descriptive statistics for the SH sample

	V_{MA}	V_{MEC}	$L_{EACcomplete}$	A_{EAC}	A_{TM}	$R_{AD(entrance)}$	$R_{AD(exit)}$	L_{AD}	$M_M + M_I$	L_M/L_I	M_S	A_{FP}
	cm^3	cm^3	mm	mm^2	mm^2	mm	mm	mm	mg		mg	mm^2
SH Cr. 4 right	4.2	0.7	28.9	39.4[a]	69.3	3.5	2.8	4.8	52.7[b]	1.2[b]	1.2	2.6
SH Cr. 4 left	3.7	0.9	26.8	39.4[a]	75.8	3.8	2.8	4.8	52.7[b]	1.2[b]	1.2	2.6
SH reference sample (*n* = 7)												
Mean	3.8	0.6	26.0	39.4	73.0	3.3	2.9	5.2	52.7[b]	1.2[b]	1.2	2.6
s. d.	2.5	0.1	2.1	13.1	4.6	0.2	0.2	0.9				0.4
Minimum	1.0	0.5	22.6	22.8	66.5	3.1	2.6	3.9				2.1
Maximum	8.8	0.7	28.5	62.2	79.2	3.6	3.3	6.6				3.1

Abbreviations: V_{MA} = volume of mastoid cells; V_{MEC} = volume of the middle ear cavity; $L_{EACcomplete}$ = complete length of the external auditory canal (EAC); A_{EAC} = area of the cross-section of the EAC; A_{TM} = area of the tympanic membrane; $R_{AD(entrance)}$ = radii of the area of the aditus at the entrance from the tympanic cavity; $R_{AD(exit)}$ = radii of the exit of the aditus to the mastoid antrum; L_{AD} = length of the aditus; $M_M + M_I$ = combined mass of the malleus and incus; L_M/L_I = middle ear lever ratio; M_S = mass of the stapes; A_{FP} = area of the stapes footplate

[a] This value is equivalent to the mean of the SH reference sample and is considered to represent the non-pathological EAC in SH Cr.4.

[b] Quam et al. (2015)

Table 4

Sound power transmission values (dB)[a] at the entrance to the cochlea for SH Cr.4 and the descriptive statistics for the SH sample.

	Frequency (kHz)							
Specimen/Sample	0.125	0.25	0.5	1.0	2.0	3.0	4.0	5.0
Cr.4 right pathological	-11.4	-4.9	2.3	13.2	10.5	10.6	2.9	-7.6
Cr.4 right normal	-11.4	-4.9	2.2	13.0	11.6	10.5	2.3	-7.1
Cr.4 left pathological	-11.7	-5.1	2.0	13.3	9.9	9.4	3.5	-8.3
Cr.4 left normal	-11.7	-5.1	2.0	13.1	10.3	9.6	4.0	-7.5
SH reference sample (*n* = 7)								
Mean	-12.1	-5.5	1.7	12.8	10.3	9.2	3.5	-4.8
Minimum	-14.5	-7.9	-0.4	11.3	8.8	7.6	-2.8	-6.9
Maximum	-10.9	-4.3	3.2	14.5	11.5	10.8	7.3	-3.4

[a]The reference value at the entrance to the outer ear is $P_0 = 10^{-18}$ W.

Supplementary Online Material (SOM):

A revision of the conductive hearing loss in Cranium 4 from the Middle Pleistocene site of Sima de los Huesos (Burgos, Spain)

Mercedes Conde-Valverde[a,*], Manuel Rosa[a,b], Ignacio Martínez[a,c], Julio Marchamalo[a], Ana Pantoja-Pérez[c], Rolf Quam[a,c,d,e], Carlos Lorenzo[f,g], Ana Gracia-Téllez[c,h], Alfredo García-Fernández[a,i,j], Juan Luis Arsuaga [a,c,k], Teresa Rivera-Rodríguez[a,l,m,n]

[a] *Cátedra de Otoacústica Evolutiva y Paleoantropología (Hospitales Madrid-Universidad de Alcalá), Departamento de Ciencias de la Vida, Universidad de Alcalá, Campus Universitario, Ctra. Madrid-Barcelona km 33,600, 28871 Alcalá de Henares, Madrid, Spain*

[b] *Departamento de Teoría de la Señal y Comunicaciones, Escuela Politécnica Superior, Universidad de Alcalá, Campus Universitario, 28805 Alcalá de Henares, Spain*

[c] *Centro Mixto (UCM-ISCIII) de Evolución y Comportamiento Humanos, Av. Monforte de Lemos 5, 28029 Madrid, Spain*

[d] *Department of Anthropology, Binghamton University (SUNY) Binghamton, NY 13902-6000 USA*

[e] *Division of Anthropology, American Museum of Natural History, Central Park West-79th St., New York, NY 10024, USA*

[f] *Àrea de Prehistòria, Departament d'Història i Història de l'Art, Universitat Rovira i Virgili, Av. Catalunya 35, 43002 Tarragona, Spain*

[g] *Institut Català de Paleoecologia Humana i Evolució Social, Campus Sescelades URV, Zona Educacional 4, 43007 Tarragona, Spain*

[h] *Área de Paleontología, Departamento de Geografía y Geología, Facultad de Ciencias, Universidad de Alcalá, Campus Universitario, Ctra. Madrid-Barcelona km 33,600, 28871 Alcalá de Henares, Madrid, Spain*

[i] *Departamento de Ciencias Médicas Clínicas, Facultad de Medicina, Universidad CEU San Pablo, Urbanización Montepríncipe, 28925 Alcorcón, Madrid, Spain.*

[j] *Hospital Universitario HM Puerta del Sur, Avda. de Carlos V 70, 28938 Móstoles, Madrid, Spain.*

[k] *Departamento de Geodinámica, Estratigrafía y Paleontología, Facultad de Ciencias Geológicas, Universidad Complutense de Madrid, 28040 Madrid, Spain*

[l] *Servicio de Otorrinolaringología, Hospital Universitario Príncipe de Asturias, Ctra. Alcalá-Meco s/n, 28805 Alcalá de Henares, Madrid, Spain*

[m] *Departamento de Cirugía, Ciencias Morfológicas y Sociales, Facultad de Medicina, Universidad de Alcalá, Campus Universitario, Ctra. Madrid-Barcelona km 33,600, 28871 Alcalá de Henares, Madrid, Spain*
[n] *Centro de Investigación Biomédica en Red en enfermedades raras (Ciberer). Instituto de Salud Carlos III (ISCIII), Monforte de Lemos, 3-5, 28029, Madrid, Spain*

* Corresponding author.
E-mail address: mercedes.conde@fgua.es (M. Conde-Valverde).

SOM S1

Analysis of sensitivity of the model

We performed an analysis of sensitivity of the model to determine the influence of the individual variables on the model results above 2 kHz (SOM Table S1). Sensitivity is related to the difference in the value for sound power at the entrance to the cochlea (in dB) obtained by increasing and decreasing the individual anatomical variable or electrical parameter by 50%. Sensitivity has been classified into three broad groupings: low (≤1dB difference), medium (>1 to ≤3dB difference), and high (>3 dB difference).

Regarding the skeletal variables which can be measured or estimated in fossil specimens, the model has a high sensitivity to the length (L_{EAC}) and cross-sectional area (A_{EAC}) of the external auditory canal, the middle ear lever ratio (L_I/L_M) and the area of the tympanic membrane (A_{TM}). The model results show a medium sensitivity to the masses of the malleus and incus ($M_I + M_M$) and the area of the stapes footplate (A_{FP}). The mass of the stapes (M_S), the volumes of the tympanic cavity (V_{MEC}) and mastoid antrum and connected air spaces (V_{MA}) and the aditus ad antrum variables (L_{AD}, R_{AD}), all show only a weak influence (low sensitivity) on the model results. In general, variables of the outer ear and ear ossicles have a stronger influence on the model results, while the middle ear spaces (tympanic cavity, mastoid antrum and air cells and aditus ad antrum) have a much weaker influence on the results.

SOM S2

Model Description

We have relied on a slightly modified version of the electrical circuit model published by Rosowski (1991, 1996) to estimate the sound power transmission through the outer and middle ears in the SH fossils. The model incorporates nearly 30 variables related to head size and the dimensions and physical properties of the anatomical structures of the outer and middle ears. The model results reflect the transmission of the sound power from the surrounding environment to the inner ear. The model accurately estimated the sound power transmission in humans, cats and chinchillas, species with considerable differences in ear dimensions and anatomy. Details of the model can be found in Quam et al. (2015) and are provided here in brief.

The electrical parameters used in the model are associated with anatomical structures of the ear (SOM Table S1). Some of these parameters are related to skeletal structures accessible in fossils, while others are related to soft tissues which are not preserved in fossil specimens. We have measured or accurately estimated in the SH specimens all of the skeletal variables included in the model (SOM Table S1). Since

the model requires values for all the variables, the respective value for modern humans has been used for the remaining soft-tissue related variables which cannot be measured in fossil specimens. This has the result of holding the soft tissue variables constant across individuals. Thus, the only source of variation in the ear measurements, and the subsequent sound power transmission values, are related to the skeletal structures of the outer and middle ear.

Although the model results are not a true audiogram, there is a strong correlation between sound power transmission through the outer and middle ear and auditory sensitivity to different frequencies (Relkin, 1988; Rosowski, 1991; Dallos, 1996). Indeed, the results for sound power transmission in modern humans and chimpanzees agree with the published audiograms for these species (Martínez et al., 2004, 2013; Quam et al., 2015). Thus, it is reasonable to conclude that the skeletal differences between humans and chimpanzees can explain an important part of the interspecific differences in their patterns of sound power transmission in the outer and middle ear. Therefore, these skeletal differences can be used to approach the sound power transmission pattern in closely-related fossil human species. This model has been previously applied to reconstruct the auditory capacities in the Middle Pleistocene hominins from the Sima de los Huesos in the Sierra de Atapuerca in northern Spain (Martínez et al., 2004, 2013).

SOM Text S3

Intraobserver and interobserver measurement error

The effects of intraobserver and interobserver measurement error on the model results for sound power transmission were reported previously in Quam et al. (2015). One *Homo sapiens* individual (CSJ 26) was virtually reconstructed and measured twice by the same researcher. The measurements are very similar in both reconstructions, and the resultant sound power transmission values from 0.5-5.0 kHz differed by a maximum of 1.6 dB at 5.0 kHz (SOM Table S2; SOM Fig. S1).

In addition, one chimpanzee (*Pan troglodytes*) individual (HTB 3434) was reconstructed twice by two different researchers. Again, the measurements are very similar in both reconstructions (SOM Table S3), and the resultant sound power transmission values from 0.5–4.0 kHz differed by <1 dB. The differences were higher at 4.5 and 5.0 kHz, but this is primarily related to a slight displacement of the point of minimum sensitivity (SOM Fig. S2).

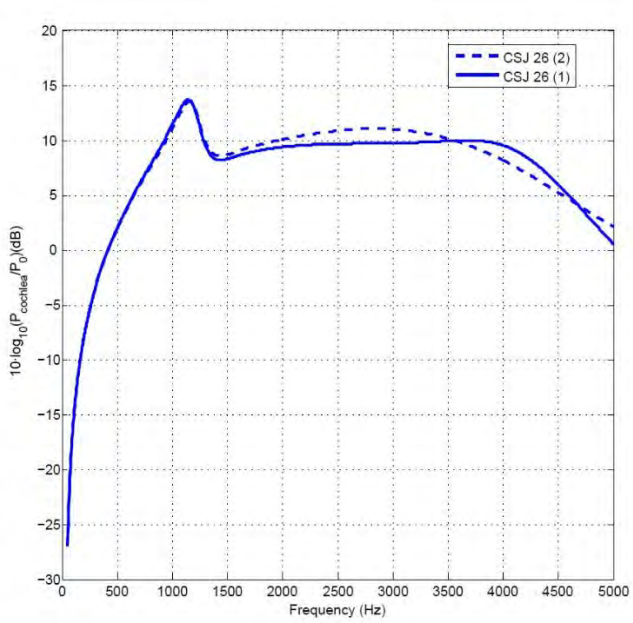

SOM Figure S1. Sound power (dB) at the entrance to the cochlea relative to $P_0=10^{-18}$ w for an incident plane wave intensity of 10^{-12} w/m^2 in two reconstructions of the CSJ 26 *H. sapiens* individual.

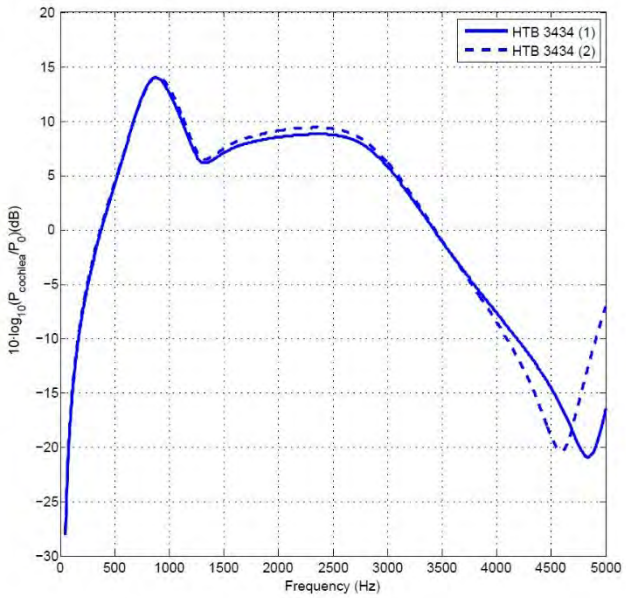

SOM Figure S2. Sound power (dB) at the entrance to the cochlea relative to $P_0=10^{-18}$ w for an incident plane wave intensity of 10^{-12} w/m^2 in two reconstructions of the HTB 3434 *P. troglodytes* individual.

Table S1

Sensitivity analysis of the model for the anatomical variables used to calculate the sound power transmission for frequencies above 2kHz.[a]

Definition	Value Used	Sensitivity (≥ 2kHz)
Ear canal length	Measured as $L_{EACcomplete}$	High (A)
Cross-sectional area of the ear canal	Measured as A_{EAC}	High (A)
Volume of the middle ear cavity	Measured as V_{MEC}	Low (A)
Volume of the mastoid air spaces	Measured as V_{MA}	Low (A)
Length and radius of the aditus ad antrum	Measured as L_{AD}, $R_{AD(entrance)}$ and $R_{AD(exit)}$	Low (E)
Area of the tympanic membrane	Measured as A_{TM}	High (A)
Functional lengths of the incus and malleus	Measured as L_I / L_M	High (A)
Masses of the incus and malleus	Measured as $M_I + M_M$	Medium (A)
Mass of the stapes	Measured as M_S	Low (A)
Area of the stapes footplate	Measured as A_{FP}	Medium (A)

[a] Anatomical variables abbreviations as in Figure 1 and Table 2 (modified from Martínez et al., 2004).

Table S2

Measurements and model results for the influence of intraindividual measurement error in *H.* sapiens.[a]

	V_{MA}	V_{MEC}	L_{AD}	$R_{AD(exit)}$	$R_{AD(entrance)}$	A_{TM}	L_{EAC}	A_{EAC}
CSJ 26 (1)	6.58	0.47	3.7	2.4	2.9	60.7	21.8	33.5
CSJ 26 (2)	6.95	0.46	4.7	2.0	2.7	57.9	22.8	33.9
Difference	-0.37	0.01	-1.0	0.4	0.2	2.8	-1.0	-0.5

Sound Power at the entrance to the Cochlea (dB)

	Frequency (KHz)					
	0.5	1.0	2.0	3.0	4.0	5.0
CSJ 26 (1)	2.0	11.4	9.4	9.7	9.5	0.5
CSJ 26 (2)	2.0	11.1	10.1	11.0	8.2	2.1
Difference	0.1	0.3	-0.7	-1.3	1.4	-1.6

[a] Modified from Quam et al. (2015). Abbreviations: V_{MA} = volume of mastoids cells (cm^3); V_{MEC} = volume of the middle ear cavity (cm^3); L_{AD} = length of the aditus (mm); $R_{AD(exit)}$ = radius of the exit of the aditus to the mastoid antrum (mm); $R_{AD(entrance)}$ = radius of the entrance to the aditus from the middle ear cavity (mm); A_{TM} = area of the tympanic membrane (mm^2); L_{EAC} = length of the external auditory canal (mm); A_{EAC} = area of the cross-section of the external auditory canal (mm^2).

Table S3

Measurements and model results for the influence of interindividual measurement error in *Pan troglodytes*.[a]

	VMA	VMEC	LAD	RAD1	RAD2	ATM	LEAC	AEAC
HTB 3434 (1)	8.06	0.35	6.2	1.9	2.3	84.3	39.8	23.0
HTB 3434 (2)	10.31	0.41	6.1	2.1	2.6	82.2	39.0	24.3
Difference	-2.25	-0.07	0.2	-0.2	-0.2	2.1	0.8	-1.3

Sound Power at the entrance to the Cochlea (dB)

	Frequency (kHz)					
	0.5	1.0	2.0	3.0	4.0	5.0
HTB 3434 (1)	4.2	12.6	8.5	5.8	-7.7	-16.5
HTB 3434 (2)	4.4	13.0	9.1	6.2	-8.5	-7.1
Difference	-0.2	-0.4	-0.6	-0.4	0.8	-9.5

[a] Modified from Quam et al. (2015). Abbreviations: V_{MA} = volume of mastoids cells (cm^3); V_{MEC} = volume of the middle ear cavity (cm^3); L_{AD} = length of the aditus (mm); $R_{AD(exit)}$ = radius of the exit of the aditus to the mastoid antrum (mm); $R_{AD(entrance)}$ = radius of the entrance to the aditus from the middle ear cavity (mm); A_{TM} = area of the tympanic membrane (mm^2); L_{EAC} = length of the external auditory canal (mm); A_{EAC} = area of the cross-section of the external auditory canal (mm^2).

SOM References

Aibara, R., Welsh, J., Puria, S., Goode, R., 2001. Human middle-ear sound transfer function and cochlear input impedance. Hearing Research 152, 100-109.

Dallos, P., 1996. Overview: Cochlear neurobiology. In: Dallos, P., Popper, A., Fay, R., (Eds.), The Cochlea. Springer-Verlag, New York, pp. 1-43.

Martínez, I., Rosa, M., Arsuaga, J., Jarabo, P., Quam, R., Lorenzo, C., Gracia, A., Carretero, J., Bermúdez de Castro, J., Carbonell, E., 2004. Auditory capacities in Middle Pleistocene humans from the Sierra de Atapuerca in Spain. Proceedings of the National Academy of Sciences USA 101, 9976-9981.

Martínez, I., Rosa, M., Quam, R., Jarabo, P., Lorenzo, C., Bonmatí, A., Gómez-Olivencia, A., Gracia, A., Arsuaga, J., 2013. Communicative capacities in Middle Pleistocene humans from the Sierra de Atapuerca in Spain. Quaternary International 295, 94-101.

Quam, R., Martínez, I., Rosa, M., Bonmatí, A., Lorenzo, C., de Ruiter, D.J., Moggi-Cecchi, J., Valverde, M.C., Jarabo, P., Menter, C.G., 2015. Early hominin auditory capacities. Science advances 1, e1500355.

Relkin, E., 1988. Introduction to the analysis of middle-ear function. In: Jahn, A., Santos-Sacchi, J., (Eds.), Physiology of the Ear. Raven, New York, pp. 103-123.

Rosowski, J., 1991. The effects of external and middle ear filtering on auditory threshold and noise-induced hearing loss. The Journal of the Acoustical Society of America 90, 124-135.

Rosowski, J., 1996. Models of external- and middle-ear function. In: Hawkins, H., McMullen, T., Popper, A., Fay, R., (Eds.), Auditory Computation. Springer, New York, pp. 15-61.